

# Networks with many structural scales: a Renormalization Group perspective

Anna Poggialini,<sup>1,2</sup> Pablo Villegas,<sup>2,3,\*</sup> Miguel A. Muñoz,<sup>4,3</sup> and Andrea Gabrielli<sup>2,5,6</sup>

<sup>1</sup>*Dipartimento di Fisica Università “Sapienza”, P.le A. Moro, 2, I-00185 Rome, Italy.*

<sup>2</sup>*‘Enrico Fermi’ Research Center (CREF), Via Panisperna 89A, 00184 - Rome, Italy*

<sup>3</sup>*Instituto Carlos I de Física Teórica y Computacional, Univ. de Granada, E-18071, Granada, Spain.*

<sup>4</sup>*Departamento de Electromagnetismo y Física de la Materia, Universidad de Granada, Granada 18071, Spain*

<sup>5</sup>*Dipartimento di Ingegneria Civile, Informatica e delle Tecnologie Aeronautiche, Università degli Studi “Roma Tre”, Via Vito Volterra 62, 00146 - Rome, Italy.*

<sup>6</sup>*Istituto dei Sistemi Complessi (ISC) - CNR, Rome, Italy.*

Scale invariance profoundly influences the dynamics and structure of complex systems, spanning from critical phenomena to network architecture. Here, we propose a precise definition of scale-invariant networks by leveraging the concept of a constant entropy loss rate across scales in a renormalization-group coarse-graining setting. This framework enables us to differentiate between scale-free and scale-invariant networks, revealing distinct characteristics within each class. Furthermore, we offer a comprehensive inventory of genuinely scale-invariant networks, both natural and artificially constructed, demonstrating, e.g., that the human connectome exhibits notable features of scale invariance. Our findings open new avenues for exploring the scale-invariant structural properties crucial in biological and socio-technological systems.

The network paradigm effectively captures essential attributes of real-world complex systems, offering a natural framework for studying entangled interconnected systems across disciplines like neuroscience [1], ecology [2], and epidemiology [3], among others [4]. Understanding the evolutionary dynamics of complex networks, as they adapt their connectivity patterns to achieve diverse goals, is crucial to understanding their long-term stability or other features influencing functional roles and performance [5, 6]. Notably, amidst the multitude of potential network structures, one organization ubiquitously arises in natural systems: the scale-free architecture [7–10].

Scale-free networks manifest a distribution of node connectivities  $k$  that decays as a power-law  $P(k) \propto k^{-\gamma}$  for large values of  $k$  [7, 11]. In statistical physics, power-law behavior is the hallmark of scale invariance and scaling behavior, implying no significant characteristic value of the analyzed quantity [12–14]. For scale-free networks, there is no typical scale in the degree of connectivity apart from natural cut-offs. However, the network community has been intrigued by the possibility of discerning, through careful statistical analyses [11, 15], including finite-size effects [16], whether empirical networks genuinely exhibit *bona-fide* scale invariance or only appear to. From a theoretical standpoint, addressing this question calls for designing a renormalization group (RG) approach [17–20]. In this framework, a fixed point of the RG transformation denotes a state or system whose characteristics remain unchanged under appropriate scale transformations achieved through iterated coarse-graining. RG fixed points are inherently linked to universal scaling laws governing the system, so systems at the same fixed point share identical scal-

ing features and belong to the same universality class [18, 20]. Hence, a key implication of RG theory is the categorization of numerous seemingly disparate physical systems and dynamical models into a relatively compact set of universality classes at criticality, either in or out of thermal equilibrium [21, 22]. Elucidating the relevant ingredients that give rise to a particular universality class offers valuable insights into the fundamental mechanisms underpinning complex systems and their key features.

Given the lack of a natural Euclidean embedding for complex networks, traditional length-scale transformations using translational invariance were deemed unfeasible until recently [23, 24]. In particular, small-world effects, characterized by short path lengths between nodes, further complicate block identification or affine transformations [24–27]. Nevertheless, various techniques have been proposed to tile the network, exploiting specific scale-invariant properties as a function of the number of links along any shortest path between two nodes [23]. These include box-covering techniques [27, 28], spectral partitioning [29], and hyperbolic geometry embeddings, which offer a promising novel approach for understanding particular complex network structures and dynamics [30, 31]. However, fully characterizing scale-invariant properties in real networks remains an open challenge.

A novel approach, the Laplacian Renormalization Group (LRG), generalizes statistical mechanics RG to graphs, providing a comprehensive framework for coarse-graining heterogeneous systems in both real and momentum space [32]. This approach uses diffusive dynamics on networks to gradually remove the smallest fine-grained structural scales, eliminating the contribution from large eigenvalues. Specifically, the LRG allows for the redefinition of effective time-dependent Laplacian and adjacency matrices at coarser scales. Due to its general validity, it comes natural to explore structural scale in-

---

\* pablo.villegas@cref.it

variance within the LRG framework, as evidenced by the observation of a time-independent rate of entropy loss [32, 33]. This leads to the fundamental question of whether non-Euclidean architectures, like general networks, can be intrinsically scale-invariant. Two key questions arise. Can we identify benchmark classes of network architectures exhibiting genuine scale-invariant behavior and, thus, define an analog to universality classes? Can we detect and quantify this kind of self-similarity in real-world networks? Here, we provide a clear definition and compilation of scale-invariant networks, emphasizing that scale-freeness, i.e., a power law degree distribution, does not imply structural self-similarity, and vice versa. Finally, we analyze actual brain networks and highlight their scale-invariant features.

### Laplacian Renormalization Group (LRG).

The introduction of a multi-scale statistical mechanical approach, the LRG, allows the detection of different scales within a network [32, 34]. The LRG is based on the time-evolution operator  $e^{-\tau\hat{L}}$  of the diffusion or heat equation, where  $\hat{L} = \hat{D} - \hat{A}$  is the Laplacian operator,  $\hat{A}$  is the adjacency matrix, and  $\hat{D}$  is the degree matrix [35]. Using this operator and denoting the Laplacian eigenvalues as  $\lambda_i$  with  $i = 1, \dots, N$  (all real and positive [36, 37]), one can define the Laplacian density matrix [38],

$$\hat{\rho}(\tau) = \frac{e^{-\tau\hat{L}}}{Z \equiv \text{Tr}(e^{-\tau\hat{L}})} = \frac{e^{-\tau\hat{L}}}{\sum_{i=1}^N e^{-\lambda_i\tau}}, \quad (1)$$

and develop a "canonical" description of heterogeneous networks in analogy with statistical mechanics [32, 35]. Here,  $\hat{L}$  formally acts as a Hermitian Hamiltonian,  $Z(\tau)$  is the partition function, and  $\tau$  serves as a control scale parameter akin to the inverse temperature. In this way, as the resolution scale  $\tau$  is increased, the contribution of large eigenvalues to  $\hat{\rho}(\tau)$ —revealing fine structure—is progressively removed, allowing for an effective network coarse-graining [39]. Within this formalism, one can compute the network entropy as  $S(\tau) = -\text{Tr}[\hat{\rho}(\tau) \log \hat{\rho}(\tau)]$ , so that  $S(\tau) = \tau \langle \lambda \rangle_\tau + \ln Z(\tau)$ , where  $\langle \lambda \rangle_\tau \equiv \langle \hat{L} \rangle_\tau = \frac{\sum_{i=1}^N \lambda_i e^{-\tau\lambda_i}}{Z(\tau)}$ . In particular,  $S$  runs from  $S = \ln N$  at  $\tau = 0$ , the segregated (*high temperature*) regime to  $S = 0$  at  $\tau \rightarrow \infty$ , the integrated (*low temperature*) regime. More specifically, one can define the network entropic susceptibility or "heat capacity" [35]

$$C(\tau) \equiv -\frac{dS}{d \log \tau}, \quad (2)$$

which describes the rate of entropy loss—i.e., the rate at which the complexity of the network shrinks upon coarse-graining—or the rate of information acquired about the network structure during diffusion dynamics at scale  $\tau$ . Recalling statistical physics, peaks of  $C$  (diverging in the infinite size limit) are associated with structural phase transitions. Thus, we can analyze  $C$  at varying  $\tau$  to investigate the network multi-scale organization, detecting

scales where entropy changes more significantly due to structural transitions. This description permitted, e.g., the detection of the network information core and its related structural/diffusive transitions [35] and led to naturally extending the RG to heterogeneous networks [32]. Here, it allows us to define informationally *scale-invariant networks* as graphs whose entropy-loss rate  $C(\tau)$  takes a constant value  $C_0 > 0$  across scales or, at least, within a sufficiently broad diffusion-time interval, thus being (exactly or approximately) scale invariant.

We demonstrate that this definition of informational scale-invariance holds if and only if the Laplacian spectral density follows  $w(\lambda) \sim \lambda^\gamma$ , considering the spectral density as a continuum distribution in the infinite network-size limit. Using Eq.(2) and the definition of  $S(\tau)$  one derives  $C(\tau) = -\tau^2 \frac{d\langle \lambda \rangle_\tau}{d\tau}$ , and setting  $C(\tau) = C_0$  as a constant, one gets  $\langle \lambda \rangle_\tau = C_0/\tau$ . The only solution to this equation is a Laplacian spectral density  $w(\lambda) \sim \lambda^\gamma$ , which allows expressing  $C_0$  as a function of the exponent  $\gamma$ , specifically  $C_0 = \gamma + 1$ . This implies that macroscopic properties—stemming from vanishing Laplacian eigenvalues—of a network with a power-law spectrum remain invariant under LRG scale transformations. Thus, network scale-invariance shifts from a power-law degree distribution to a power-law in the spectral density. Note that the exponent of the Laplacian spectral density,  $\gamma$ , can be related to the *spectral dimension*,  $d_s$ , which is a global property of the graph, related, e.g., to the infrared singularity of the Gaussian process [40] and that has been shown to provide a robust generalization of the standard dimension for networks [40, 41]. As  $d_s/2 = \gamma + 1$  [40], one concludes that  $C_0$  is constant and equals half of the graph's spectral dimension:  $C_0 = d_s/2$ . Thus, measuring the plateau value of the heat capacity of a scale-invariant network effectively determines its dimensionality.

For finite-sized networks, scale invariance may only be approximate and confined to a finite-scale interval. This means that  $C(\tau)$  cannot remain constant across all scales: it decays from its plateau value  $C_0$  to 0 for sufficiently large values of  $\tau$ . To estimate this cut-off, we have to consider that the smallest non-zero eigenvalue  $\lambda_2$  of  $\hat{L}$ , also called "spectral gap" or "Fiedler eigenvalue"  $\lambda_F$ , [42, 43], is the one providing the slowest decaying contribution in time to Eq.(1), therefore determining the asymptotic time decay of  $C(\tau)$ . Starting from Eq.(2) and imposing that the Laplacian spectrum  $\omega(\lambda)$  integrates to  $N$ , we get  $\lambda_F \sim N^{-2/d_s}$  for large  $N$  [44, 45]. From this, it follows (see Supplemental Material, SM [46]),

$$C\left(\frac{\alpha}{\lambda_F}\right) \simeq \frac{\Gamma\left(\frac{d_s}{2}\right) \Gamma\left(\frac{d_s}{2} + 2, \alpha\right) - \Gamma^2\left(\frac{d_s}{2} + 1, \alpha\right)}{\Gamma^2\left(\frac{d_s}{2}\right)}, \quad (3)$$

where  $\Gamma(x, \alpha) = \int_\alpha^\infty du u^{x-1} e^{-u}$  is the lower incomplete Euler Gamma function which exponentially decreases in  $\alpha$  for  $\alpha \gg 1$ , with  $\alpha$  a free parameter. This allows a complementary way to estimate  $d_s$  from finite-size scaling of

$C(\tau)$  in finite scale-invariant networks. For practical purposes, this can be done by studying the scaling in  $N$  of  $\tau$  in the large time-decaying region for which  $C$  gets a fixed value. We use  $C = 1/2$ , referred to as  $\tau_F$ .

**Laplacian Random-Walk RG.** The LRG method relies on a "heat-like" diffusion process defined by  $\hat{L}$ . However, we wonder whether the results obtained for scale-invariance and graph dimensionality remain valid when using the Laplacian random-walk operator,  $\hat{L}_{RW} = \hat{D}^{-1}\hat{L}$  instead of  $\hat{L}$ .  $\hat{L}_{RW}$  describes the time-discrete dynamics of a RW moving from a node to a neighbor with uniform probability and represents the transition matrix for RW dynamics on a graph [36, 47]. Although  $\hat{L}_{RW}$  is not symmetric, it is equivalent to the symmetric operator  $\hat{L}_{sym} = D^{1/2}\hat{L}_{RW}\hat{D}^{-1/2}$  [36] with all its eigenvalues real and satisfying  $0 \leq \mu_i \leq 2$ . We can, thus, reformulate the LRG for the RW dynamics by substituting  $\hat{L}$  with  $\hat{L}_{sym}$ , renaming the related heat capacities as  $C_L$  and  $C_{RW}$ , respectively. In fact,  $\hat{L}_{RW}$  provided the original definition of the RW spectral dimension,  $d_s^{RW}$ , related to the first-return time distribution of the random-walker  $P_0(t)$  [40, 48] by the scaling  $P_0(t) \propto t^{-d_s^{RW}/2}$ . This extends the behavior on  $d$ -dimensional lattices where  $P_0(t) \propto t^{-d/2}$  [49]. While  $\hat{L}$  or  $\hat{L}_{RW}$  strictly coincide in regular networks like lattices, both operators unravel heterogeneous network structures in different ways [34] and, to our knowledge, there is no proof that  $d_s = d_s^{RW}$  for generic heterogeneous networks.

**LRG non-trivial fixed points.** Subsequently, we tackle the following lingering questions: What are the current non-trivial fixed points of the LRG, i.e., families or "universality classes" of scale-invariant networks? Are scale-invariant networks necessarily scale-free? Do results depend on the choice of the operator?

Let us remark that regular lattices, with a degree distribution  $P(\kappa) = \delta(\kappa - \kappa_0)$ , represent the simplest case of scale-invariant structures lacking scale-free properties (see SM [46]). However, our main focus is categorizing *heterogeneous* and *stochastic* scale-invariant networks.

The **first** category of self-similar networks comprises trees, i.e., connected loopless networks. It is known that the spectral dimension of random trees, with minimal branching ratio  $b_{min} = 1$ , depends upon the first two moments of the degree distribution  $P(\kappa)$  [50, 51]. Specifically,  $d_s = 4/3$  if  $\langle \kappa^2 \rangle$  is finite, while the problem remains open when  $\langle \kappa^2 \rangle$  diverges [50, 52, 53]. Here, we examine specific cases within these two classes, with the lenses of LRG: ordinary random trees (RT) and Barabási-Albert (BA) networks where new nodes attach preferentially to existing ones, forming  $m = 1$  edges [7]. As reported in Fig.1(a),  $C_L$  shows a plateau corresponding to the theoretically known spectral dimension for random trees,  $d_s^{RT} = 4/3$  [52] and follows the finite-size scaling condition, Eq.(3). Also, we observe that  $\hat{L}_{RW}$  does not alter this value (see Fig.1(b)), despite specific differences in the shape of  $C$ , as the local peak at short times in Fig.1(b).

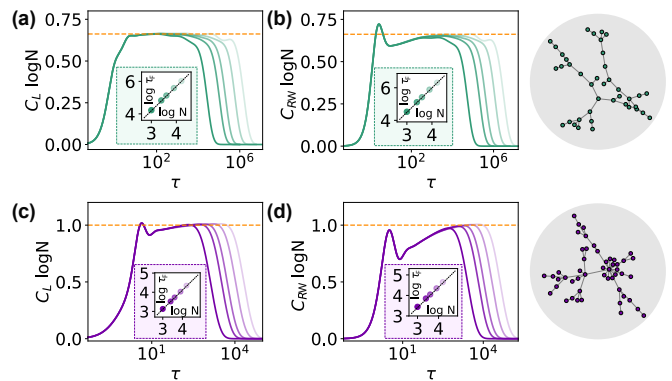


Figure 1. **Trees.** Heat capacity versus diffusion time for: (a)-(b) Random trees and (c)-(d) Barabasi-Albert networks with  $m = 1$ . We have used  $\hat{L}$  in (a) and (c) and  $\hat{L}_{RW}$  in (b) and (d). Insets show the scaling of  $\tau_F$  as a function of the network size  $N$ . Orange dashed lines and solid black lines represent the theoretical expectation,  $d_s^{RT} = 4/3$  and  $d_s^{BA} = 2$ . All curves have been averaged over  $10^3$  independent realizations. Different colors represent different sizes  $N = \{1, 2.5, 4, 8, 16\} \times 10^3$ .

Instead, BA networks with  $m = 1$  are trees with diverging  $\langle \kappa^2 \rangle$ . As shown in Fig.1(c), they have a constant heat capacity  $C_L$  corresponding to a spectral dimension  $d_s = 2$ . Although  $C_{RW}$  grows in the intermediate regime, it also becomes flat for asymptotic times and large network sizes (see Fig.1), confirming scale-invariance with  $d_s^{RW} = d_s = 2$ . This same spectral dimension is also obtained for Bethe lattices with coordination number  $z \geq 3$  (see [54] and SM [46]). Furthermore, BA networks with  $m > 1$  show no sign of scale invariance (see SM [46]), proving that the archetypes of scale-free networks are not scale-invariant. This prevents preferential attachment from generating self-similar networks with  $d_s > 2$ .

**Second**, we consider networks that, contrary to trees, have a non-vanishing clustering coefficient. In particular, the Dorogovstev-Golstev-Mendes [55] networks and their generalization:  $(u, v)$ -flowers [24, 55, 56]. These deterministic fractal-like structures grow by iteratively replacing the link between two nodes with two paths of lengths  $u$  and  $v$  (see SM [46]). Diameter-based analyses, such as calculating the Hausdorff dimension of these networks lead to an apparent paradox: all  $(1, v)$  flowers are infinite-dimensional and exhibit anomalous scaling functions [24, 55, 57]. This paradox stems from the lack of network embedding in an Euclidean space. Conversely, as shown in Figs.2(a), (b) and SM [46], all flowers exhibit well-defined spectral dimensions [24],  $d_s = \log(u + v)/\log(uv)$  changing from  $d_s \approx 3.17$  to  $d_s = 1$ . Fig.2(b) sheds light on their differences:  $(u, v)$  flowers with  $u > 1$  exhibit characteristic oscillations emerging from the discrete nature of the recursive network growth process (much as log-periodic oscillations in standard

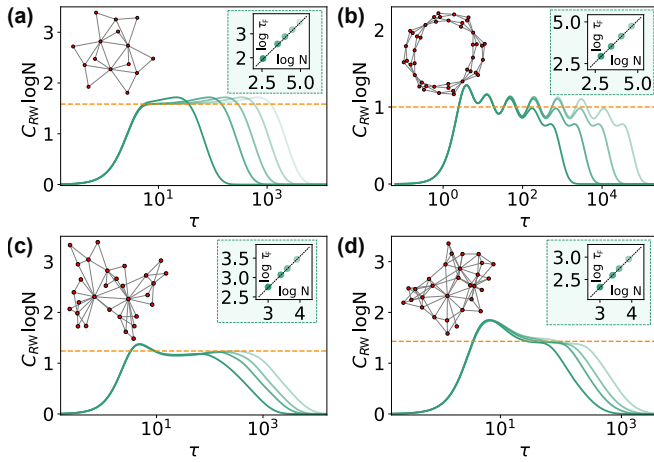


Figure 2. **Clustered networks.** RW heat capacity versus diffusion time for: (a) (1, 2) flowers with  $s = 6, 8, 9, 10$  and 11, hierarchical levels (b) (2, 2) flowers with  $s = 5, 6, 7$ , and 8. For  $(u, v)$  flowers, the number of nodes is  $N_s = \left(\frac{w}{w-1} + \frac{w-2}{w-1}w^s\right)$ , with  $w = u + v$ . (c) KH with  $m = 2$  and (d) KH with  $m = 3$  of sizes  $N = \{1, 2.5, 4, 8\} \times 10^3$ . Insets show the scaling  $\tau_F$  as a function of the system size. Orange dashed lines and solid black lines represent the theoretical expectation. All curves have been averaged over  $10^3$  independent realizations.

fractal analyses of deterministic structures, as stem from their discrete-scale invariance [13, 58]). Thus, we demonstrate that the method detects the presence of discrete scale invariance on networks.

**Third,** to explore whether self-similarity can exist in stochastic scale-free graphs with small-world properties [24], we consider the Kim and Holme (KH) model [59]. This requires modifying BA networks by introducing a probability  $p$  for each newly added node to form a triangle with existing nodes (see SM [46]). The resulting networks show a power-law degree distribution with high clustering coefficient. LRG analysis of KH networks reveals scale-invariance only when  $p = 1$ . As shown in Figs.2(c) and (d),  $C_{RW}$  (and  $C_L$  [46]) shows a plateau with spectral dimension from  $d_s = 2.57(1)$  to  $d_s = 3.65(1)$  as  $m$  increases (see SM [46]).

**Fourth,** we have investigated the behavior of networks with a built-in hierarchical structure. In particular, we have analyzed the Dyson graph [60, 61]: a fully-connected deterministic graph with hierarchically organized link weights, resulting in a tunable spectral dimension  $d_s = 2/(2\sigma - 1)$  where  $\sigma$  is a scaling parameter controlling the weight strength at every scale (see SM [46]). Fig.3(a) shows the constant plateau of  $C_L$  for a Dyson network with  $\sigma = 0.85$ , consistent with the theoretical value. We have also examined hierarchical modular networks (HMNs) that were proposed using inspiration from actual brain networks [62]. In HMNs, nodes grouped in basal fully-connected modules are recursively coupled with nodes in other moduli, establishing inter-modular

links randomly in a hierarchical fractal-like manner (see SM [46]). Fig.3(b) shows their heat capacity: HMNs are scale-invariant for any set of parameters, with spectral dimension in the range  $d_s \in (1.25, 2)$  (see SM [46]).

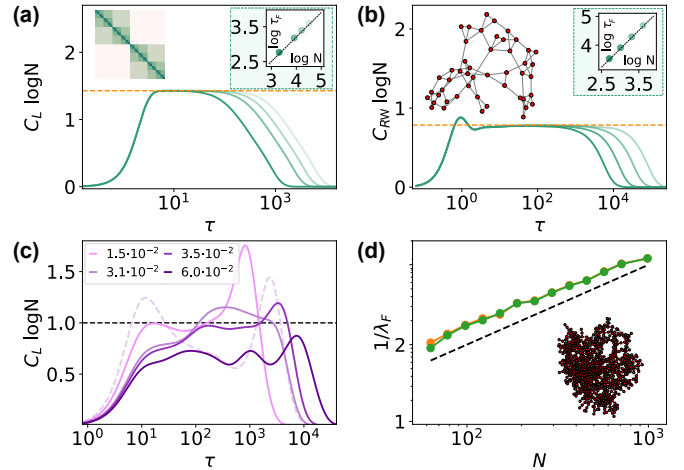


Figure 3. **Hierarchical networks.** Heat capacity versus diffusion time for: (a) Dyson graphs with  $\sigma = 0.85$  and  $s = 11, 13, 14, 15$  hierarchical levels. The network size is  $N = 2^s$  in both cases. The upper left inset shows the weighted adjacency matrix. (b) HMNs with  $m_0 = 3$  and  $\alpha = 2$  (see SM [46]) for  $s = 9, 10, 11, 12$  hierarchical levels ( $N = 2^s m_0$ ). Insets show the scaling of  $\tau_F$  as a function of  $N$ . Orange dashed and solid black lines represent the theoretical expectation. (c) The HC for different thresholds (see legend). (d) The scaling of  $\tau_F$  for coarse-grained versions of the HC with  $T = 3 \cdot 10^{-2}$  and different fixed values of  $\tau = 10^{-1}, 10^0$ , and  $10^1$ . Black dashed line corresponds to  $d_s = 1.9$ .

**Finally,** we have analyzed the Human Connectome (HC) structural brain network [1] (see SM [46]). The analysis of  $C_L$  for the largest available (thresholded) HC network is shown in Fig.3(c), while Fig.3(d) shows the finite-size scaling of  $\lambda_F$  for reduced versions of the HC. Both analyses support an underlying scale-invariant topology with spectral dimension  $d_s \sim 1.9(1)$ .

**Outlook.** The observation of scale-invariance across length and time scales led to the development of RG ideas [18, 20] whose initial implementation took advantage of the geometrical homogeneity and translational invariance to perform scaling of statistical physical systems, computing critical exponents [63], and leading to a categorization of apparently diverse phase transitions into a few universality classes [21, 22].

Extending universality to networks with heterogeneous and non-local connectivity properties has long challenged physicists. Despite remarkable advances have been recently made [27, 28, 30, 31, 64], fully understanding scale-invariance in generic networks remains unresolved. Initially, network scale-invariance was associated with power-law degree distributions [16]. However, as we explicitly show, *scale-freeness* of node degrees is neither necessary nor sufficient for true self-similarity [11]. In-

stead, the LRG [32, 35], provides a general framework to characterize and classify *non-trivial* structural LRG fixed points, describing their scaling properties and offering a classification in terms of universality classes. A constant heat-capacity indicates the presence of scale-invariance or self-similarity in graphs, characterized by a constant entropy-loss rate during network coarse-graining. We have linked the constant entropy-loss rate to the network spectral dimension,  $d_s$ —computed using either  $\hat{L}$  or  $\hat{L}_{RW}$ —confirming its role as a natural generalization of the Euclidean dimension [40, 41, 48].

Our LRG analysis identifies regular lattices, trees, clustered networks, and hierarchical networks as fundamental classes of scale-invariant networks. Beyond regular lattices, we highlight (u-v)-flowers and KH networks as unique structures combining local clustering with hubs at all scales to generate self-similar topologies. Trees are bound to  $d_s \leq 2$ , and simply adding hubs appears insufficient to achieve higher-dimension values. Generally, as the dimension increases, it becomes more challenging to generate self-similar heterogeneous networks [24]. Our findings are promising for studying biological and socio-technological networks; notably, hierarchical networks, including the HC [65, 66] which exhibit robust scale invariance with  $d_s \approx 1.9(1)$ , corroborating previous results [64]. Our findings provide a solid ground for future dynamical RG theoretical calculations on these structures and for identifying new signatures of scale invariance in real-world networks.

#### ACKNOWLEDGMENTS

The authors thank T.Gili, D. Cassi, and R. Burioni for very useful discussions and comments. P.V. and M.A.M. acknowledge financial support from the Spanish "Ministerio de Ciencia, Innovación y Universidades" and the "Agencia Estatal de Investigación (AEI)" under Project Ref. PID2020-113681GB-I00 funded by MICIN/AEI/10.13039/501100011033.

- 
- [1] A. Fornito, A. Zalesky, and E. Bullmore, *Fundamentals of brain network analysis* (Academic press, 2016).
- [2] J. Bascompte, *Basic Appl. Ecol.* **8**, 485 (2007).
- [3] R. Pastor-Satorras and A. Vespignani, *Phys. Rev. Lett.* **86**, 3200 (2001).
- [4] M. E. Newman, *SIAM Rev.* **45**, 167 (2003).
- [5] M. A. Fortuna, J. A. Bonachela, and S. A. Levin, *Proc. Natl. Acad. Sci. U.S.A.* **108**, 19985 (2011).
- [6] P. Villegas, M. A. Muñoz, and J. A. Bonachela, *J. R. Soc. Interface.* **17**, 20190845 (2020).
- [7] A.-L. Barabási and R. Albert, *Science* **286**, 509 (1999).
- [8] M. Newman, *Networks: An Introduction* (Oxford University Press, Oxford, 2010).
- [9] A. Barabási, *Network Science* (Cambridge University Press, Cambridge, 2016).
- [10] G. Caldarelli, A. Capocci, P. De Los Rios, and M. A. Muñoz, *Phys. Rev. Lett.* **89**, 258702 (2002).
- [11] A. D. Broido and A. Clauset, *Nat. Comm.* **10**, 1017 (2019).
- [12] M. E. Newman, *Contemp. Phys.* **46**, 323 (2005).
- [13] D. Sornette, *Critical phenomena in natural sciences: chaos, fractals, selforganization and disorder: concepts and tools* (Springer-Verlag Berlin, Heidelberg, 2006).
- [14] M. A. Muñoz, *Rev. Mod. Phys.* **90**, 031001 (2018).
- [15] A. Clauset, C. R. Shalizi, and M. E. Newman, *SIAM Rev.* **51**, 661 (2009).
- [16] M. Serafino, G. Cimini, A. Maritan, A. Rinaldo, S. Suweis, J. R. Banavar, and G. Caldarelli, *Proc. Natl. Acad. Sci. U.S.A.* **118**, e2013825118 (2021).
- [17] K. G. Wilson, *Sci. Am.* **241**, 158 (1979).
- [18] D. J. Amit and V. Martin-Mayor, *Field Theory, the Renormalization Group, and Critical Phenomena*, 3rd ed. (World Scientific, Singapore, 2005).
- [19] G. Caldarelli, A. Gabrielli, T. Gili, and P. Villegas, *J. Stat. Mech.: Theory Exp.* **2024**, 084002 (2024).
- [20] M. Kardar, *Statistical physics of fields* (Cambridge University Press, Cambridge, 2007).
- [21] P. C. Hohenberg and B. I. Halperin, *Rev. Mod. Phys.* **49**, 435 (1977).
- [22] G. Ódor, *Rev. Mod. Phys.* **76**, 663 (2004).
- [23] F. Radicchi, J. J. Ramasco, A. Barrat, and S. Fortunato, *Phys. Rev. Lett.* **101**, 148701 (2008).
- [24] H. D. Rozenfeld, S. Havlin, and D. Ben-Avraham, *New J. Phys.* **9**, 175 (2007).
- [25] R. Cohen and S. Havlin, *Phys. Rev. Lett.* **90**, 058701 (2003).
- [26] D. J. Watts and S. H. Strogatz, *Nature* **393**, 440 (1998).
- [27] H. D. Rozenfeld, C. Song, and H. A. Makse, *Phys. Rev. Lett.* **104**, 025701 (2010).
- [28] C. Song, S. Havlin, and H. A. Makse, *Nature* **433**, 392 (2005).
- [29] D. Gfeller and P. De Los Rios, *Phys. Rev. Lett.* **99**, 038701 (2007).
- [30] M. A. Serrano, D. Krioukov, and M. Boguñá, *Phys. Rev. Lett.* **100**, 078701 (2008).
- [31] G. García-Pérez, M. Boguñá, and M. Á. Serrano, *Nat. Phys.* **14**, 583 (2018).
- [32] P. Villegas, T. Gili, G. Caldarelli, and A. Gabrielli, *Nat. Phys.* **19**, 445–450 (2023).
- [33] K. Klemm, *Nat. Phys.* **19**, 318 (2023).
- [34] P. Villegas, A. Gabrielli, A. Poggialini, and T. Gili, arXiv (2023), 2301.04514.
- [35] P. Villegas, A. Gabrielli, F. Santucci, G. Caldarelli, and T. Gili, *Phys. Rev. Research* **4**, 033196 (2022).
- [36] F. R. Chung, *Spectral graph theory*, Vol. 92 (American Mathematical Soc., Providence, 1997).
- [37] L. Donetti, F. Neri, and M. A. Muñoz, *J. Stat. Mech.: Theory Exp.* **2006**, P08007 (2006).
- [38] M. De Domenico and J. Biamonte, *Phys. Rev. X* **6**, 041062 (2016).
- [39] This idea is also at the basis of different existing community detection algorithms [34, 67–69].
- [40] R. Burioni and D. Cassi, *Phys. Rev. Lett.* **76**, 1091 (1996).
- [41] D. Cassi, *Phys. Rev. Lett.* **68**, 3631 (1992).
- [42] M. Fiedler, *Banach Center Publications* **1**, 57 (1989).
- [43] F. Chung, L. Lu, and V. Vu, *Proc. Natl. Acad. Sci. USA* **100**, 6313 (2003).
- [44] K. C. Das, *Comput. Math. Appl.* **48**, 715 (2004).
- [45] S. N. Dorogovtsev and J. F. Mendes, *The nature of complex networks* (Oxford University Press, 2022).

- [46] See Supplemental Material at [].
- [47] R. Burioni and D. Cassi, *J. Phys. A* **38**, R45 (2005).
- [48] D. Cassi and L. Fabbian, *J. Phys. A* **32**, L93 (1999).
- [49] S. Alexander and R. Orbach, *J. Phys. Lett.* **43**, 625 (1982).
- [50] L. Donetti and C. Destri, *J. Phys. A Math. Gen.* **37**, 6003 (2004).
- [51] Z. Burda, J. D. Correia, and A. Krzywicki, *Phys. Rev. E* **64**, 046118 (2001).
- [52] C. Destri and L. Donetti, *J. Phys. A Math. Gen.* **35**, 9499 (2002).
- [53] S. N. Dorogovtsev, A. V. Goltsev, J. F. Mendes, and A. N. Samukhin, *Phys. Rev. E* **68**, 046109 (2003).
- [54] A. Erzan and A. Tuncer, *Linear Algebra Its Appl.* **586**, 111–129 (2020).
- [55] S. N. Dorogovtsev, A. V. Goltsev, and J. F. F. Mendes, *Phys. Rev. E* **65**, 066122 (2002).
- [56] H. D. Rozenfeld, L. K. Gallos, C. Song, and H. A. Makse, “Fractal and transfractal scale-free networks,” in *Encyclopedia of Complexity and Systems Science*, edited by R. A. Meyers (Springer, New York, 2009) pp. 3924–3943.
- [57] J. Peng and E. Agliari, *Chaos* **27**, 083108 (2017).
- [58] T. Vicsek, M. Shlesinger, and M. Matsushita, *Fractals in Natural Sciences* (World Scientific, Singapore, 1994).
- [59] P. Holme and B. J. Kim, *Phys. Rev. E* **65**, 026107 (2002).
- [60] F. J. Dyson, *Commun. Math. Phys.* **12**, 91 (1969).
- [61] E. Agliari and F. Tavani, *Sci. Rep.* **7**, 39962 (2017).
- [62] P. Moretti and M. A. Muñoz, *Nat. Comm.* **4**, 2521 (2013).
- [63] K. G. Wilson and M. E. Fisher, *Phys. Rev. Lett.* **28**, 240 (1972).
- [64] M. Zheng, A. Allard, P. Hagmann, and M. Á. Serrano, *Proc. Natl. Acad. Sci. USA* **117**, 20244 (2020).
- [65] O. Sporns, D. R. Chialvo, M. Kaiser, and C. C. Hilgetag, *Trends Cogn. Sci.* **8**, 418 (2004).
- [66] P. Hagmann, L. Cammoun, X. Gigandet, R. Meuli, C. J. Honey, V. J. Wedeen, and O. Sporns, *PLoS Biol.* **6**, e159 (2008).
- [67] A. Arenas, A. Díaz-Guilera, and C. J. Pérez-Vicente, *Phys. Rev. Lett.* **96**, 114102 (2006).
- [68] L. Donetti and M. A. Muñoz, *J. Stat. Mech.: Theory Exp.* **2004**, P10012 (2004).
- [69] L. Donetti, P. I. Hurtado, and M. A. Muñoz, *Phys. Rev. Lett.* **95**, 188701 (2005).

# Supplemental Material: Networks with many structural scales: a Renormalization Group perspective

Anna Poggialini,<sup>1,2</sup> Pablo Villegas,<sup>2,3,\*</sup> Miguel A. Muñoz,<sup>4,3</sup> and Andrea Gabrielli<sup>2,5</sup>

<sup>1</sup>*Dipartimento di Fisica Università “Sapienza”, P.le A. Moro, 5, I-00185 Rome, Italy.*

<sup>2</sup>*‘Enrico Fermi’ Research Center (CREF), Via Panisperna 89A, 00184 - Rome, Italy*

<sup>3</sup>*Instituto Carlos I de Física Teórica y Computacional,*

*Universidad de Granada, E-18071, Granada, Spain.*

<sup>4</sup>*Departamento de Electromagnetismo y Física de la Materia, Universidad de Granada, Granada 18071, Spain*

<sup>5</sup>*Dipartimento di Ingegneria Civile, Informatica e delle Tecnologie Aeronautiche, Università degli Studi “Roma Tre”, Via Vito Volterra 62, 00146 - Rome, Italy.*

## CONTENTS

1. Asymptotic limit of $\lambda_F$	2
2. Asymptotically scale-invariant graphs	3
3. Regular lattices	3
4. Scale-dependent networks	4
5. Bethe lattices	5
6. Barabási-Albert networks	6
7. $(u, v)$ –flowers	7
8. Kim and Holme networks	9
9. Dyson network	10
10. HMN networks	11
11. Human Connectome network	13
References	14

---

\* pablo.villegas@cref.it

## 1. ASYMPTOTIC LIMIT OF $\lambda_F$

Let us assume to have a scale-invariant network for which  $\omega(\lambda) = A\lambda^\gamma$ , with  $\gamma = d_s/2 - 1$  and that  $\lambda_{max}$  do not depend on  $N$  (reasonable if the maximum node degree does not scale with  $N$ ) [1]. Since the total number of eigenvalues is  $N$ , i.e. the number of network nodes, we have

$$A \int_0^{\lambda_{max}} d\lambda \lambda^\gamma \equiv A \frac{\lambda_{max}^{\gamma+1}}{\gamma+1} = N,$$

which implies  $A = \frac{\gamma+1}{\lambda_{max}} N$ . On the other hand, by the definition of the Fiedler eigenvalue  $\lambda_F$ , we need to have [2],

$$A \int_0^{\lambda_F} d\lambda \lambda^\gamma = 1,$$

from which we can derive the scaling relation  $\lambda_F \sim N^{-2/d_s}$ .

Under these hypotheses, the specific heat can be written as

$$C(t) = t^2 \left( \langle \lambda^2 \rangle_t - \langle \lambda \rangle_t^2 \right) = t^2 \frac{\left( A \int_0^{\lambda_{max}} d\lambda \lambda^\gamma e^{-\lambda t} \right) \left( A \int_{\lambda_F}^{\lambda_{max}} d\lambda \lambda^{\gamma+2} e^{-\lambda t} \right) - \left( A \int_{\lambda_F}^{\lambda_{max}} d\lambda \lambda^{\gamma+1} e^{-\lambda t} \right)^2}{\left( A \int_0^{\lambda_{max}} d\lambda \lambda^\gamma e^{-\lambda t} \right)^2}, \quad (1)$$

where the lower integration extreme for the integrals of the first and second moments of  $\lambda$  with time dependent measure  $\hat{\rho}(t)$  is explicitly limited to  $\lambda_F$  as the fundamental eigenvalue  $\lambda = 0$  does not contribute and in this way we can explicitly study the effect of the  $N$ -dependent gap  $\lambda_F \sim N^{-2/d_s}$  for finite  $N$ .

By the change of integration variable  $u = \lambda t$ , we can write

$$C(t) = \frac{\left( \int_0^{u_{max}} du u^\gamma e^{-u} \right) \left( \int_{\lambda_F t}^{u_{max}} du u^{\gamma+2} e^{-u} \right) - \left( \int_{\lambda_F t}^{u_{max}} du u^{\gamma+1} e^{-u} \right)^2}{\left( \int_0^{u_{max}} du u^\gamma e^{-u} \right)^2} \quad (2)$$

with  $u_{max} = \lambda_{max} t$ .

Let us now evaluate  $C(t_F)$  with  $t_F = \alpha/\lambda_F \sim N^{2/d_s}$  where  $C(t)$  is expected to deviate from the constant value  $d_s/2$  because of finite size effects giving a constant gap. In this case, due to the exponential factor in the integrals, we can take with no danger  $u_{max} \rightarrow +\infty$ . Consequently, we can write

$$C(\alpha/\lambda_F) = \frac{\Gamma(\gamma+1) \int_\alpha^\infty du u^{\gamma+2} e^{-u} - \left( \int_\alpha^\infty du u^{\gamma+1} e^{-u} \right)^2}{\Gamma^2(\gamma+1)} = \frac{\Gamma(\gamma+1)\Gamma(\gamma+3, \alpha) - \Gamma^2(\gamma+2, \alpha)}{\Gamma^2(\gamma+1)}, \quad (3)$$

where  $\Gamma(x)$  is the complete Euler Gamma function and  $\Gamma(x, \alpha) = \int_\alpha^\infty du u^{x-1} e^{-u}$  is the lower incomplete Euler Gamma function. Equation (3) immediately shows that for different  $N$  we get the same large time value for the specific heat  $C(t)$ , different from the infinite  $N$  value  $d_s/2$ , at corresponding times  $t = \alpha/\lambda_F$  where  $\lambda_F \sim N^{-2/d_s}$ , while this value depends on  $\alpha$ . In particular, by using the large  $\alpha$  asymptotic expansion of  $\Gamma(x, \alpha)$  in Eq. (3) we get that the main  $\alpha$  dependence characterized by the following exponential decay:

$$C(\alpha/\lambda_F) = \frac{\alpha^{\gamma+2} e^{-\alpha}}{\Gamma(\gamma+1)}. \quad (4)$$

Finally, it is simple to note that in the limit  $\alpha \rightarrow 0^+$  Eq. (3) correctly coincides with the limit  $N \rightarrow \infty$  of Eq. (2) at finite  $t$ :

$$C(t) = \frac{\Gamma(\gamma+1)\Gamma(\gamma+3) - [\Gamma(\gamma+2)]^2}{[\Gamma(\gamma+1)]^2} = \gamma+1 = d_s/2,$$

which explains the plateau value.



## 2. ASYMPTOTICALLY SCALE-INVARIANT GRAPHS

Despite its simplicity, the request for a unique power-law behavior to hold on to all the support of the spectrum may seem too severe to be easily detected in both synthetic and real graphs. However, a large set of networks satisfies a much weaker but equally relevant condition:  $\omega(\lambda) \sim \lambda^\gamma$  in the limit  $\lambda \rightarrow 0$ . Networks that meet this asymptotic condition are scale-invariant graphs. The results shown in the main text can be derived, in a more general way, for the asymptotic case using the Tauberian and Abelian theorems [3]. In particular, one can write

$$C(t)\log(N) = -t^2 \frac{d}{dt} h(t). \quad (5)$$

If  $\omega(\lambda) \sim \lambda^\gamma$  in for  $\lambda \rightarrow 0$ , then  $h(t) \sim t^{-1}$  in the limit  $t \rightarrow \infty$  and  $C(t)\log(N) \sim \gamma + 1 < \infty$  in the same regime. In this context, the study of the spectral dimension  $d_s$  fits the well-known asymptotic definitions  $d_s = -2 \lim_{t \rightarrow \infty} \frac{\ln p_t(G,v)}{\ln t}$  and  $\lim_{\lambda_N \rightarrow 0} \omega_N(\lambda_N)$  when these limits exist for infinite-sized graphs and where  $p_t(G,v)$  is the return probability of a random walk to a generic vertex  $v$  at time  $t$  and  $\omega_N(\lambda_N)$  is the spectral density of normalized Laplacian operator.

## 3. REGULAR LATTICES

For consistency and to avoid spurious results, we first study the most straightforward trivial scale-invariant structures: regular lattices. As shown in Figure 1, the  $\tau$  peak at short diffusion times reflects the characteristic resolution scale of the system (or, in other words, the 'cutoff' scale,  $\Lambda$ ). We have analyzed different simple cases (both in 2D and 3D) to check the correspondence between the specific heat and the expected dimension of the network, using both  $\hat{L}$  and  $\hat{L}_{RW}$ . We emphasize that, in this particular case, both Laplacians are formally equivalent, as for regular lattices,  $P(\kappa) = \delta(\kappa - \kappa_0)$ , where  $k_0$  represents the coordination number of the homogeneous structure.

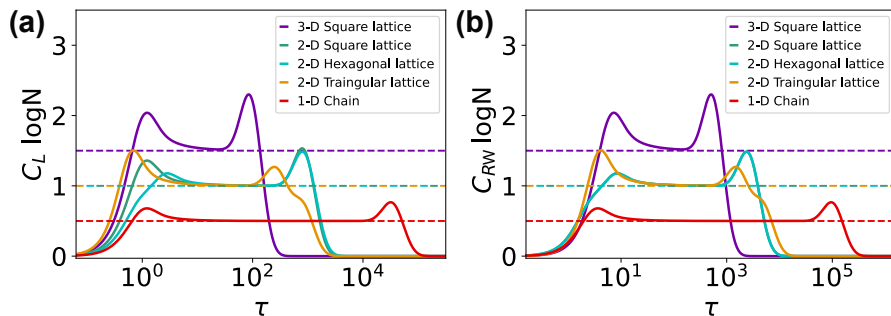


FIG. 1. **Regular lattices.** Specific heat versus diffusion time by using (a)  $\hat{L}$  and (b)  $\hat{L}_{RW}$ . All networks show a plateau for the expected dimension of any lattice for both cases.

## 4. SCALE-DEPENDENT NETWORKS

We have conducted extensive simulations to analyze the specific heat of Erdős-Rényi networks of different mean connectivity. Figure 2 shows the expected specific heat versus the diffusion time for different sizes of the system, which shows that there is no scaling for large networks. Note also that  $C_L$  presents a single peak, pointing to a scale that corresponds to the system size.

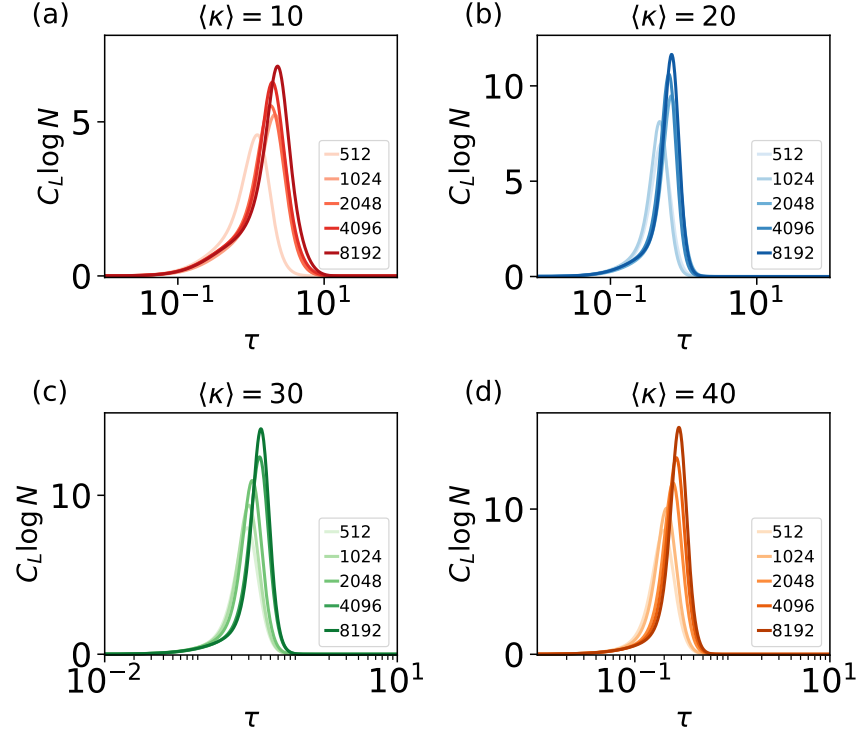


FIG. 2. **Erdős-Rényi networks.** Specific heat versus diffusion time for different network sizes (see legend) and mean connectivity: (a)  $\langle \kappa \rangle = 10$ , (b)  $\langle \kappa \rangle = 20$ , (c)  $\langle \kappa \rangle = 30$ , (d)  $\langle \kappa \rangle = 40$ . All curves have been averaged over  $10^2$  network realizations.

## 5. BETHE LATTICES

One of the paradigmatic cases of self-similar networks is those of Bethe lattices with coordination number  $z > 2$ . Figure 3 shows the specific heat for different Bethe lattices with coordination numbers  $z = 3, 4, 5$  and 6. Note that the specific heat monotonically grows for all networks at short times. Still, the heat capacity asymptotically converges to a constant value with a spectral dimension  $d_S = 2$  (see Figure 3). The scaling of the Fiedler eigenvalue confirms such a constant value (see also the theoretical proof below), as reported in Figure 4.

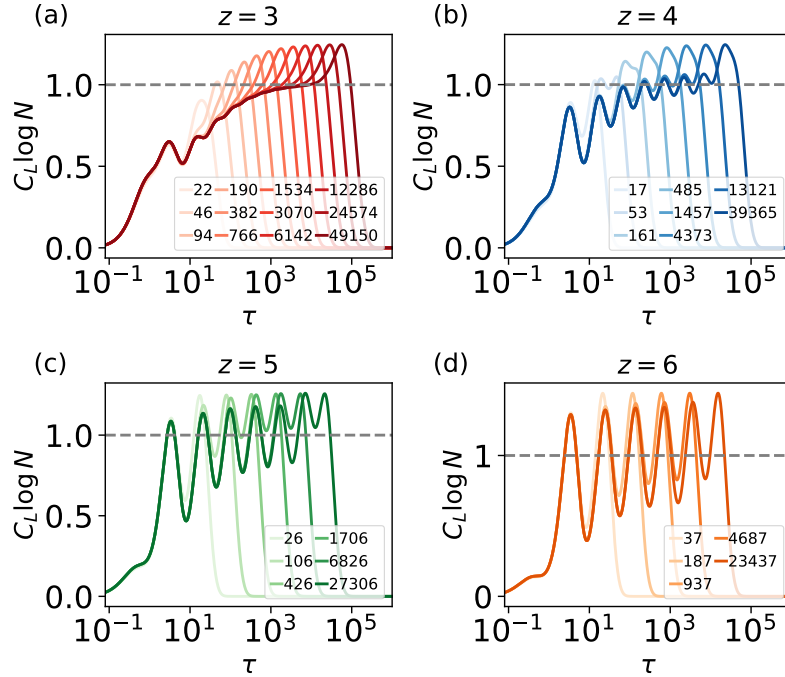


FIG. 3. **Bethe lattice.** Specific heat versus system size for Bethe lattices of different coordination numbers: (a)  $z = 3$ , (b)  $z = 4$ , (c)  $z = 5$ , (d)  $z = 6$ . The dashed gray line shows the value associated with the scaling of the Fiedler eigenvalue in Figure 4.

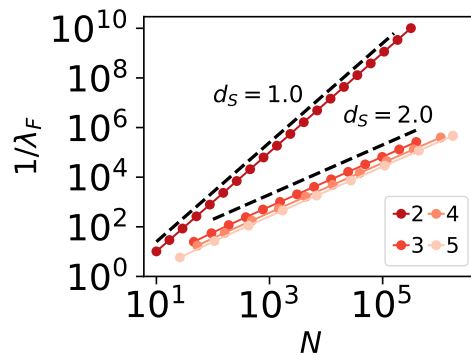


FIG. 4. **Fiedler scaling.** Scaling of the inverse of the Fiedler eigenvalue versus system size for different Bethe lattices and different values of  $z$  (see legend). Black dashed lines correspond to  $1/\lambda_F \sim N^{2/d_S}$ . Bethe lattices with  $z \geq 3$  present generic scaling with associated spectral dimension  $d_S = 2$ .

We now rigorously demonstrate that all Bethe lattices exhibit an identical spectral dimension  $d_S = 2$ . For convenience, let us consider a regular Cayley tree where all nodes present a branching ratio  $b$  and  $r$  iterations. The total number of nodes is

$$N_r = \frac{b^r - 1}{b - 1} \Rightarrow r = \frac{\log(Nb - N + 1)}{\log b}$$

Following the results of Erzan and Tuncer [4], we know that,

$$\lambda_F \sim (b - 1) b^{-r} = \frac{b - 1}{b^{\frac{\log(Nb - N + 1)}{\log b}}}$$

and thus,

$$\frac{1}{\lambda_F} \sim \frac{b^{\frac{\log(Nb - N + 1)}{\log b}}}{b - 1}$$

where the upper term simply involves the change of base formula  $\log_b a = \frac{\log_c a}{\log_c b}$ . Finally,

$$\frac{1}{\lambda_F} \sim N + \frac{1}{b - 1}$$

By comparison with the scaling form for  $1/\lambda_F$ ,  $d_S = 2$ , regardless of the value of  $b$ .

## 6. BARABÁSI-ALBERT NETWORKS

We have analyzed BA networks with subsequent values of  $m > 1$  for both cases  $\hat{L}$  and  $\hat{L}_{RW}$ . As shown in Figures 5 and 6, BA networks show no sign of scaling properties for  $m > 1$ , nor in the specific heat, where any plateau is present, nor in the analysis of the Fiedler eigenvalue, where only the network with  $m = 1$  presents a bona-fide scaling with  $d_S = 2$ .

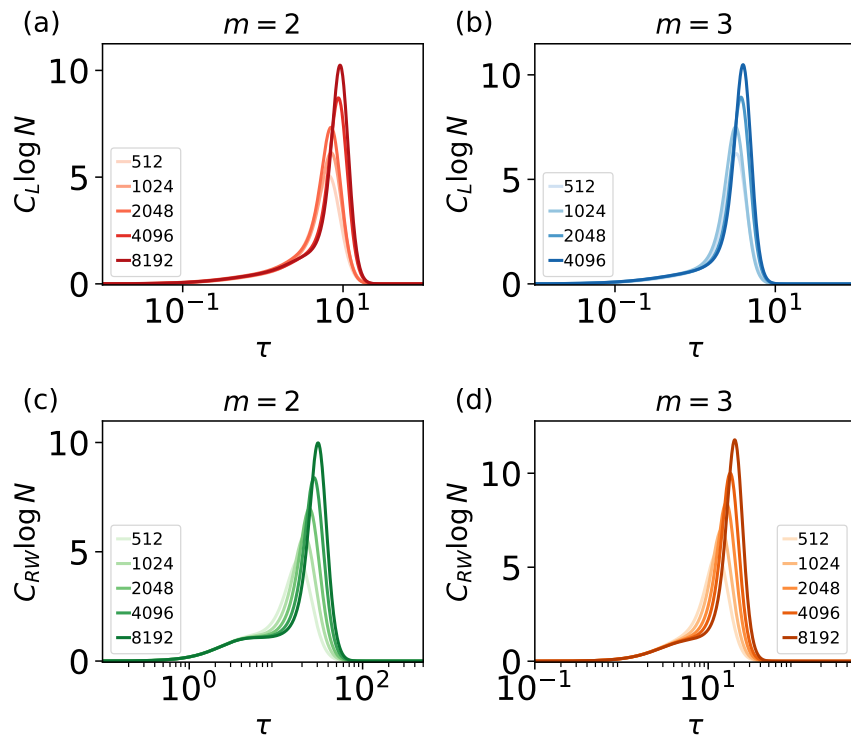


FIG. 5. **Barabási-Albert**. Specific heat versus system size for BA networks of different  $m$  for: (a)  $\hat{L}$ ,  $m = 2$ , (b)  $\hat{L}$ ,  $m = 3$ , (c)  $\hat{L}_{RW}$ ,  $m = 2$ , and (d)  $\hat{L}_{RW}$ ,  $m = 3$ . All cases show no plateau, evidencing the absence of scale-invariant properties of the networks.

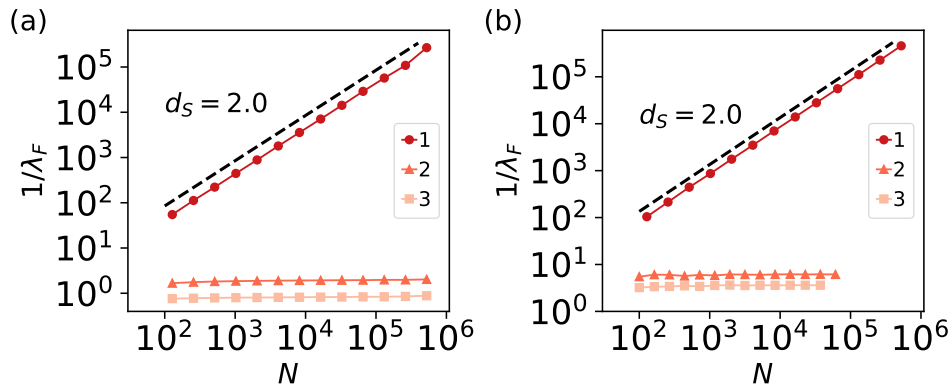


FIG. 6. **Spectral dimension.** Scaling of the inverse of the Fiedler eigenvalue versus system size for different Barabási-Albert networks and different values of  $m$  (see legend) by using (a) the Laplacian  $\hat{L}$  and (b) the normalized Laplacian  $L_{RW}$ . In both cases, only the case with  $m = 1$  is truly scale-invariant with spectral dimension  $d_s = 2$ .

### 7. $(u, v)$ -FLOWERS

The  $(u, v)$ -flowers are deterministic and recursive graphs [5]. Let us briefly describe how such networks are built: At step  $t = 0$ , the graph  $G(0)$  corresponds to a dimer, that is, two nodes connected by a link. The structure of successive  $G(t > 0)$  is driven by both the parameters  $u$  and  $v$ , together with  $1 \leq u \leq v$ .  $G(t)$  is built by replacing each link of  $G(t - 1)$  with two parallel links of, respectively, length  $u$  and  $v$ , as shown in Fig. 7.

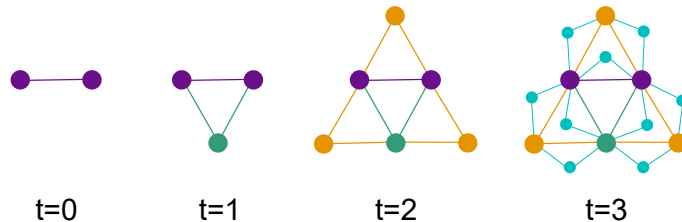


FIG. 7. Construction of the  $(1, 2)$ -flowers at steps  $t = 0, 1, 2, 3$ .

Such a procedure generates different types of graphs. Hence,  $(> 1, v)$ -flowers are known to exhibit finite Hausdorff dimension,  $d_H$ , while  $(1, v)$ -flowers have been called transfinite fractals (transfractals) and hold strong small-world properties with infinite Hausdorff dimension. In particular, all the derivations of  $d_H$  are based on rescaling analyses of the diameter of the graph  $L$  (e.g.,  $N(L + \ell) = e^{\ell \bar{d}_f} N(L)$ ,  $N$  number of nodes) instead of a multiplicative one (e.g.,  $N(bL) = b e^{d_f} N(L)$ ). However, we note that the general spectral dimension of both types of networks is  $d_s = \log(u + v) / \log(uv)$ , corresponding to the analysis of the Fiedler eigenvalue in Figure 9. Note also that, as expected for usual deterministic and recursively growing fractals [6], periodic oscillations are observed and detected by the specific heat as exemplified in Fig. 8.

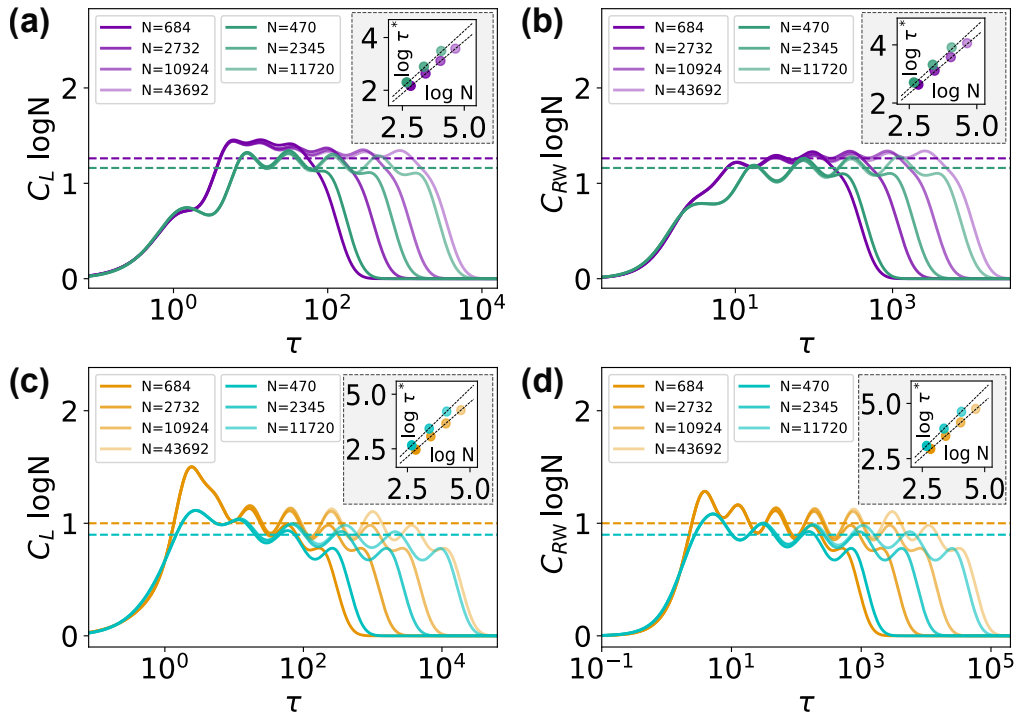


FIG. 8. **(u,v)-flowers.** Specific heat versus diffusion time  $\tau$  for different system sizes (see legend) for (1,3)-flowers (purple solid line) and (1,4)-flowers (green solid line) by using (a)  $\hat{L}$ , and (b)  $\hat{L}_{RW}$ , and (2,2)-flowers (orange solid line) and (2,3)-flowers (cyan solid line) by using (c)  $\hat{L}$  and (d)  $\hat{L}_{RW}$ . The colored horizontal dashed lines display the theoretical value of  $d_S/2$ , and the black dashed lines in the sub-panels show the theoretical scaling of  $C_F$  as suggested in the main text.

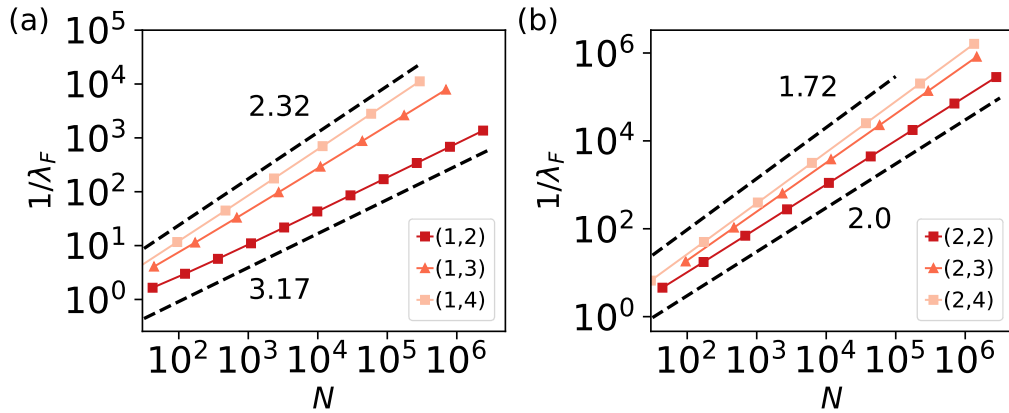


FIG. 9. **Spectral dimension for (u,v) networks.** Scaling of the inverse of the Fiedler eigenvalue versus system size for different  $(u, v)$  networks and different values of  $v$  (see legend) by using the Laplacian  $\hat{L}$  for (a)  $u = 1$ , (b)  $u = 2$ . In all cases, these networks are scale-invariant with variable spectral dimensions.

## 8. KIM AND HOLME NETWORKS

The analysis of standard BA networks with an extended mechanism to include a ‘triad formation step’ is particularly interesting to explore possible mechanisms to generate self-similar networks with  $d_S > 2$  [7]. Therefore, the generation mechanism proposed by Kim and Holme (KH) works by adding a new step to the preferential attachment rule as follows:

- (i) A vertex,  $v$ , with  $m$  edges is added at each time step. The growth time  $t$  is identified as the number of time steps.
- (ii) Preferential attachment rule (PA): Each edge of  $v$  is then linked to an already existing vertex with probability proportional to its degree, namely,  $P_i = \frac{\kappa_i}{\sum_j \kappa_j}$ .
- (iii) Triad formation (TF): After each PA step in which a new vertex  $v$  is added and some edge  $(u, v)$  is added, a triangle is closed with probability  $p$  by choosing a neighbor of  $u$ ,  $u_2$  and adding the edge  $(v, u_2)$ .

Here, we investigate whether KH networks show any power-law scaling of the Fiedler eigenvalue for different values of  $m$  and  $p$ . Let us highlight that the case with  $m = 1$  is rather trivial because it is impossible to close any triangle. Consequently, this latter mechanism will produce results identical to those of a simple BA network with  $m = 1$ . The results of the different types of KH networks (that is, the values of  $m$ ) for different TF probabilities are reported in Figure 10, making it evident that only KH networks with  $p = 1$  generate scale-invariant structures, as shown in the main text. In particular, the spectral dimension of the generated networks ranges from  $d_S = 2.57(1)$  and  $d_S = 3.65(1)$  for large values of  $m$ , as shown in Figure 11(b). Figure 11(a) and Figure 11(c) shows a specific example of these networks with  $m = 2$  and  $m = 3$ .

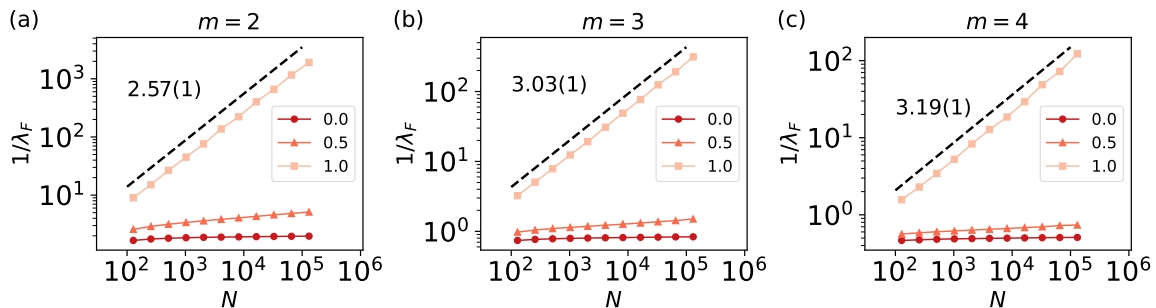


FIG. 10. **KH scale-invariant networks.** Scaling of the inverse of the Fiedler eigenvalue versus system size for different KH networks and different values of  $p$  (see legend) by using the Laplacian  $\hat{L}$  for (a)  $m = 2$ , (b)  $m = 3$ , and (c)  $m = 4$ . In all cases, only the case with  $p = 1$  is truly scale-invariant with variable spectral dimension.

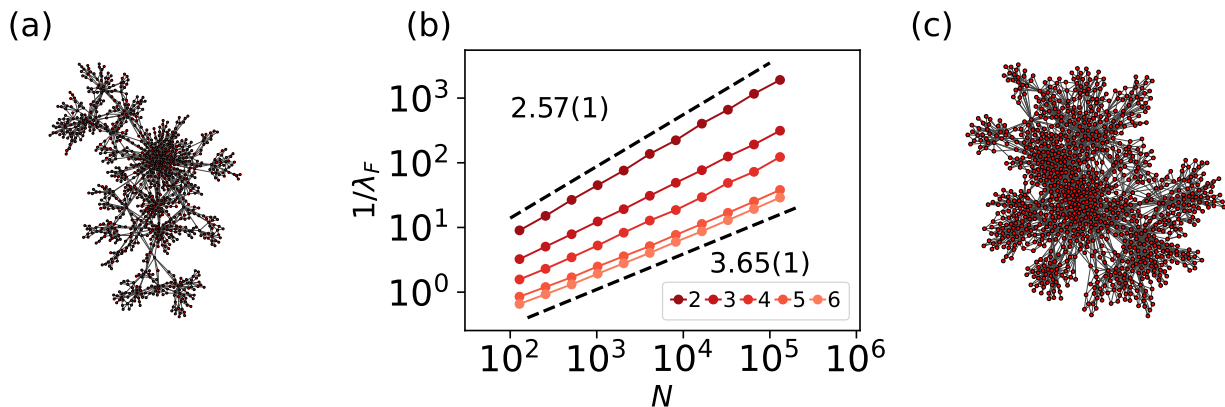


FIG. 11. **KH networks.** (a) KH network with  $m = 2$ ,  $p = 1$  and  $N = 1000$ . (b) Scaling of the inverse of the Fiedler eigenvalue versus system size for different KH networks with  $p = 1$  and varying  $m$  (see legend). The spectral dimension of the networks range from  $d_S = 2.57(1)$  to  $d_S = 3.65(1)$  for large values of  $m$ . (c) KH network with  $m = 3$ ,  $p = 1$  and  $N = 1000$ .

## 9. DYSON NETWORK

The Dyson graph is a weighted, fully connected, and deterministic graph. It was originally introduced by Dyson [8] to determine the occurrence of a phase transition in a one-dimensional chain with long-range interactions.

In the initial step, the network consists of a dimer with a weight link  $J(d = 1, t = 1, \sigma) = 4^{-\sigma}$ . Here,  $t$  is the iteration step, which is an integer  $\geq 1$ , such that the initial configuration of the dimer is called  $G(1)$ .  $d$  is the distance between two nodes and corresponds to the iteration step where they have been connected. In the next step, the graph is duplicated and all missing links are filled with a weight connection  $J(d = 2, t = 2, \sigma) = 4^{-2\sigma}$ . The same quantity is added to the weight of the old links, which now reads as  $J(d = 1, t = 2, \sigma) = J(d = 1, t = 1, \sigma) + 4^{-2\sigma}$ . Generalizing we get  $J(d, t - 1, \sigma) \rightarrow J(d, t, \sigma) = J(d, t - 1, \sigma) + J(t, t, \sigma)$ . Then it follows that each node will hold a unique degree  $w \equiv w_i = \sum_{i \neq j} J_{ij} = \sum_{d=1}^T 2^{d-1} J(d, T, \sigma)$ , where  $J(d, T, \sigma) = \sum_{l=d}^T J(l, t, \sigma)$ . Thus, the parameter  $\sigma$  can be adjusted to modulate the decay of the interaction strength. In particular, its value affects the resulting spectral dimension that can be written as  $d_S = 2/(2\sigma - 1)$ . Finally, we have to add that  $\sigma$  is bounded as follows:  $1/2 < \sigma \leq 1$ . The lower bound ensures the finite value of  $w$ . The upper bound does not let the inverse of the spectral gap grow faster than the system size.

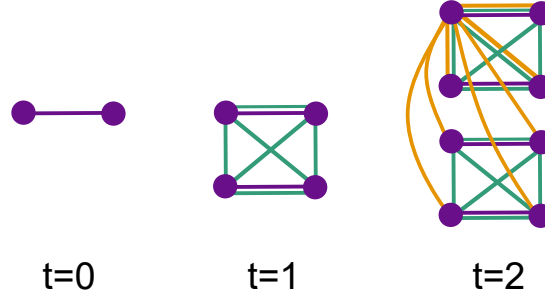


FIG. 12. Construction of Dyson graph at steps  $t = 0, 1, 2$ . For the sake of clarity, at step  $t = 2$ , only the new links involving the first node have been reported. The rest of the nodes will follow the same building rule.

Figure 13 shows the constant specific heat for different Dyson graphs with  $\sigma = 0.85$  and  $\sigma = 0.95$  and different system sizes. Note that these graphs can generate networks of arbitrary spectral dimension.

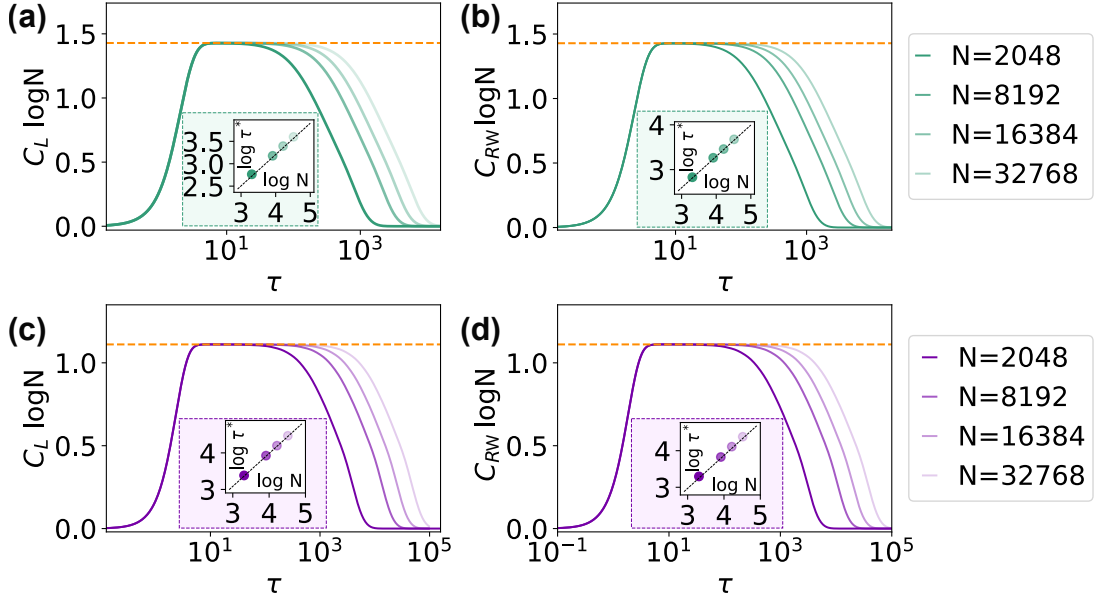


FIG. 13. **Dyson graphs.** Specific heat versus diffusion time  $\tau$  for different system sizes (see legend) for  $\sigma = 0.85$  using (a)  $\hat{L}$  and (b)  $\hat{L}_{RW}$ , and  $\sigma = 0.95$  using (c)  $\hat{L}$  and (d)  $\hat{L}_{RW}$ . The colored horizontal dashed lines display the theoretical value of  $d_S/2$ , and the black dashed lines in the sub-panels show the theoretical scaling of  $C_F$  as suggested in the main text.



## 10. HMN NETWORKS

We have also analyzed the synthetic hierarchical networks originally developed in [9]. These networks, called Hierarchic Modular Networks (HMNs), have been specifically generated to closely resemble the structure of real brain networks. In particular, HMN consists of  $N$  nodes or neurons and  $L$  links or synapses, organized into hierarchical levels for easy analysis. The HMN model that we exemplify here uses a bottom-to-top approach. First, we construct local fully connected modules and group them recursively by establishing new inter-modular links in a deterministic manner with a level-dependent number of connections (HMN).

Hence, the growing algorithm works as follows, as detailed in [9]:

- (i) At each hierarchical level  $l = 1, 2, \dots, s$ , different pairs of blocks are selected, each with size  $2^{l-1}M_0$ . All possible undirected  $4^{l-1}M_0^2$  connections between the two blocks are evaluated and established to avoid repetitions.
- (ii) The number of connections between blocks at each level is set a priori at a constant value  $\alpha$ .
- (iii) This method is stochastic in assigning connections, although the number of them (as well as the degree of the network) is fixed deterministically, being,

$$\langle \kappa \rangle = M_0 - 1 + \frac{2\alpha}{M_0}(1 - 2^{-s}).$$

Figure 14 shows the eigenvalue probability distribution for HMNs with  $M_0 = 2$  and different values of  $\alpha$ . Note the power-law scaling for small values of  $\lambda$ , where the number of oscillations increases with the number of hierarchical levels,  $s$ . Figure 15 shows the inverse of the Fiedler eigenvalue for different classes of HMN networks using fully connected cliques of size  $M_0 = 2$ ,  $M_0 = 3$ , and  $M_0 = 4$  as basal blocks. In particular, we observe that the spectral dimension of these specific networks continuously varies over the interval  $d_S \in (1.25, 2)$ .

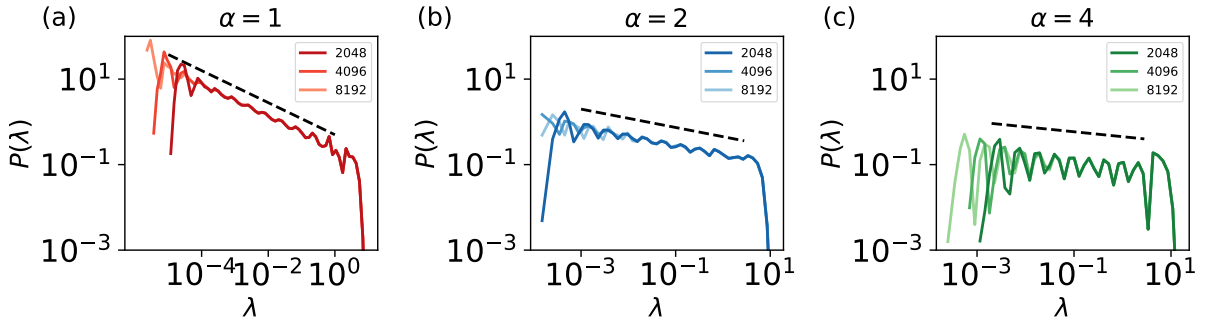


FIG. 14. **HMN eigenvalues.** Eigenvalue probability distribution for HMN networks with  $M_0 = 2$  and different system sizes (see legend) by using the Laplacian  $\hat{L}$  for (a)  $\alpha = 1$ , (b)  $\alpha = 2$ , and (c)  $\alpha = 4$ . All curves have been averaged over  $10^3$  independent realizations. Dashed lines represent the scaling  $P(\lambda) \propto \lambda^{d_S/2-1}$ .

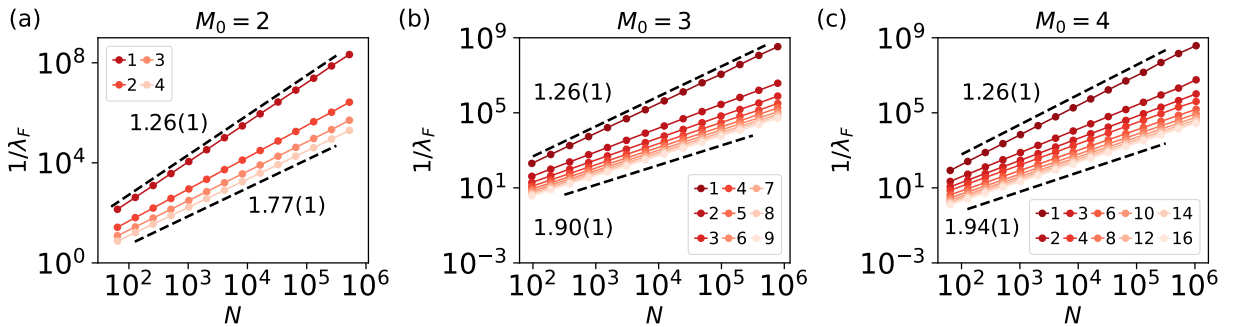


FIG. 15. **HMN spectral dimension.** Scaling of the inverse of the Fiedler eigenvalue versus system size for different HMN networks and different values of  $\alpha$  (see legend) by using the Laplacian  $\hat{L}$  for (a)  $M_0 = 2$ , (b)  $M_0 = 3$ , and (c)  $M_0 = 4$ . In all cases, HMN are scale-invariant networks with variable spectral dimensions.

Figure 16 shows the constant specific heat for different HMN networks for  $M_0 = 2$  and different values of  $\alpha$ . Note that all networks present a constant specific heat, either for  $C_L$  and  $C_R$  with the expected theoretical value of  $d_S$ .

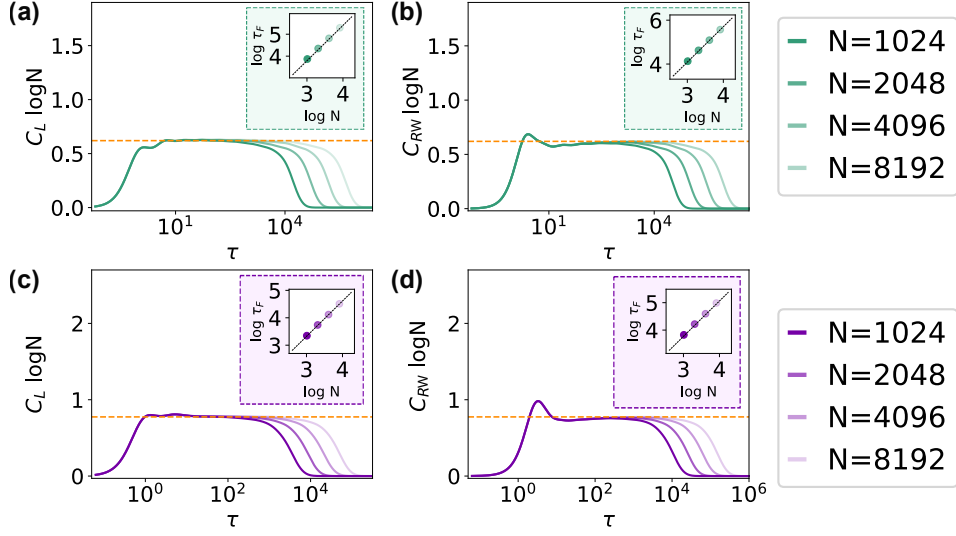


FIG. 16. **HMN graphs.** Specific heat versus diffusion time  $\tau$  for  $M_0 = 2$  and  $\alpha = 1$  using (a)  $\hat{L}$  and (b)  $\hat{L}_{RW}$ , and  $M_0 = 2$  and  $\alpha = 2$  using (c)  $\hat{L}$  and (d)  $\hat{L}_{RW}$ . The colored horizontal dashed lines display the plateau level, and the black dashed lines in the sub-panels show the theoretical scaling of  $C_F$ , as suggested in the main text. All curves have been averaged over  $10^3$  network realizations.

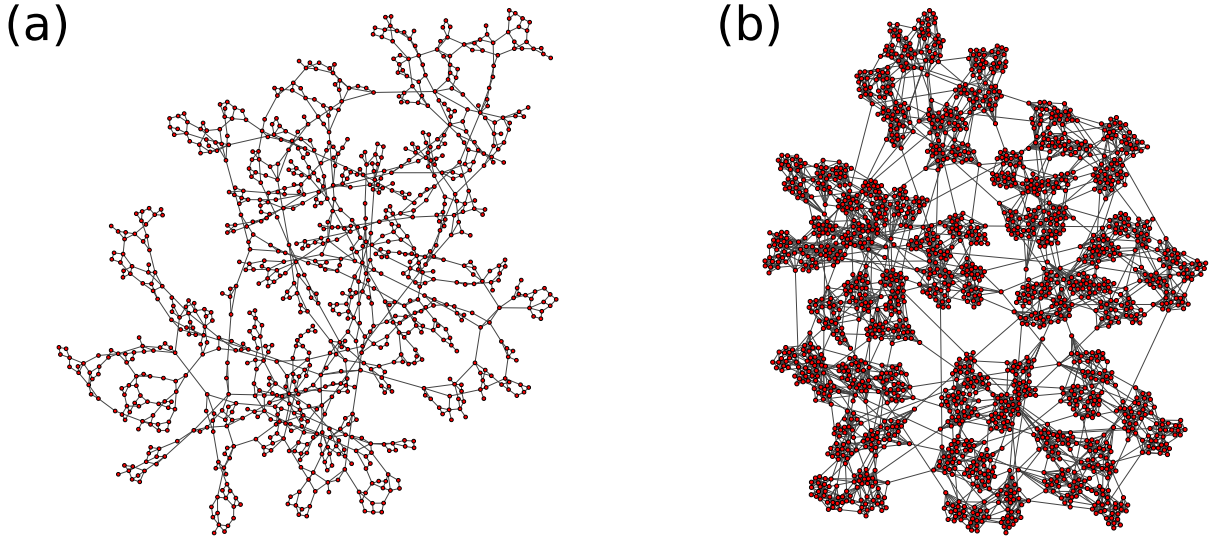


FIG. 17. **HMN networks.** (a) HMN network with  $M_0 = 2$ ,  $\alpha = 2$  and  $s = 9$  hierarchical levels. (b) HMN network with  $M_0 = 4$ ,  $\alpha = 10$  and  $s = 9$  hierarchical levels.

## 11. HUMAN CONNECTOME NETWORK

We have also analyzed the intrinsic structure of the Human Connectome Network (HC), a reconstruction of structural brain networks composed of hundreds of neural regions and thousands of white-matter fiber interconnections. This network consists of 998 nodes, each representing a mesoscopic population of neurons whose mutual connections are encoded by a symmetric weighted connectivity matrix. In particular, it is well-known that the HC is organized in modules and structured in a hierarchical fashion across many scales.

To uncover incipient scale-invariant features in HC, we have filtered the weighted HC matrix by imposing a threshold  $T$  below which the links are discarded (without performing any network binarization). We emphasize that, as a function of this threshold  $T$ , a random tree will always emerge, forming the backbone of the giant component of every network at the percolation threshold. However, here we observe that the network exhibits a kind of plateau near  $d_S \approx 2$  for  $T \in (2 \cdot 10^{-2}, 5 \cdot 10^{-2})$ , which is consistent with our previous results for HMN networks. Figure 18(a) shows the fraction of nodes belonging to the giant cluster ( $P_\infty$ ) and the remaining fraction of edges regarding their initial number ( $E_\infty$ ) when we sparsify the network. Note that at some specific value of  $T \approx 6 \cdot 10^{-2}$ , the resulting giant component corresponds to a random tree at the critical point of percolation. Instead, Figure 18(b) shows the resulting specific heat for the giant connected component of the sparsified network. Figure 19 shows the resulting networks for the different values of  $T$  analyzed in Figure 18(b).

Finally, to check whether the HC network actually exhibits scale-invariant properties, we performed iterative coarse-graining of the network using the LRG [10] and monitored the scaling of the Fiedler vector for different system sizes. We used the density matrix  $\rho(\tau)$  to define a network dendrogram as explicitly described in [10, 11]. Hence, by applying Ward's method to analyze the HC network clusters, it is possible to cut the dendrogram at different heights to generate reduced networks of smaller sizes, as shown in the main text.

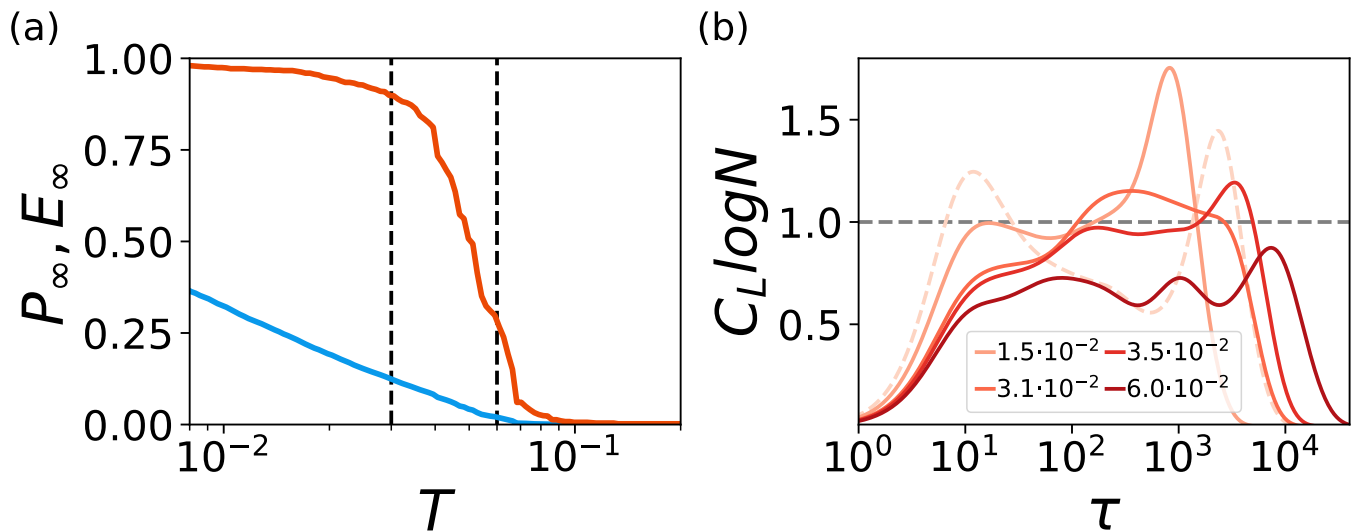


FIG. 18. (a) Giant cluster size ( $P_\infty$ ) and fraction of edges regarding the total original ones ( $E_\infty$ ) versus sparsification threshold  $T$ . The network shows a usual percolation phase transition for  $T \approx 0.6$ , while a non-trivial network structure still emerges with a non-vanishing giant component for threshold values  $T \in (2 \cdot 10^{-2}, 5 \cdot 10^{-2})$ . (b) Specific heat versus diffusion time for different values of  $T$  (see legend). Values of  $T$  within  $(2 \cdot 10^{-2}, 5 \cdot 10^{-2})$  are compatible with a spectral dimension  $d_S \approx 1.9(1)$ , while for  $T \approx 0.6$  a random tree with spectral dimension  $d_S = 4/3$  emerges, as expected for any percolation phase transition.

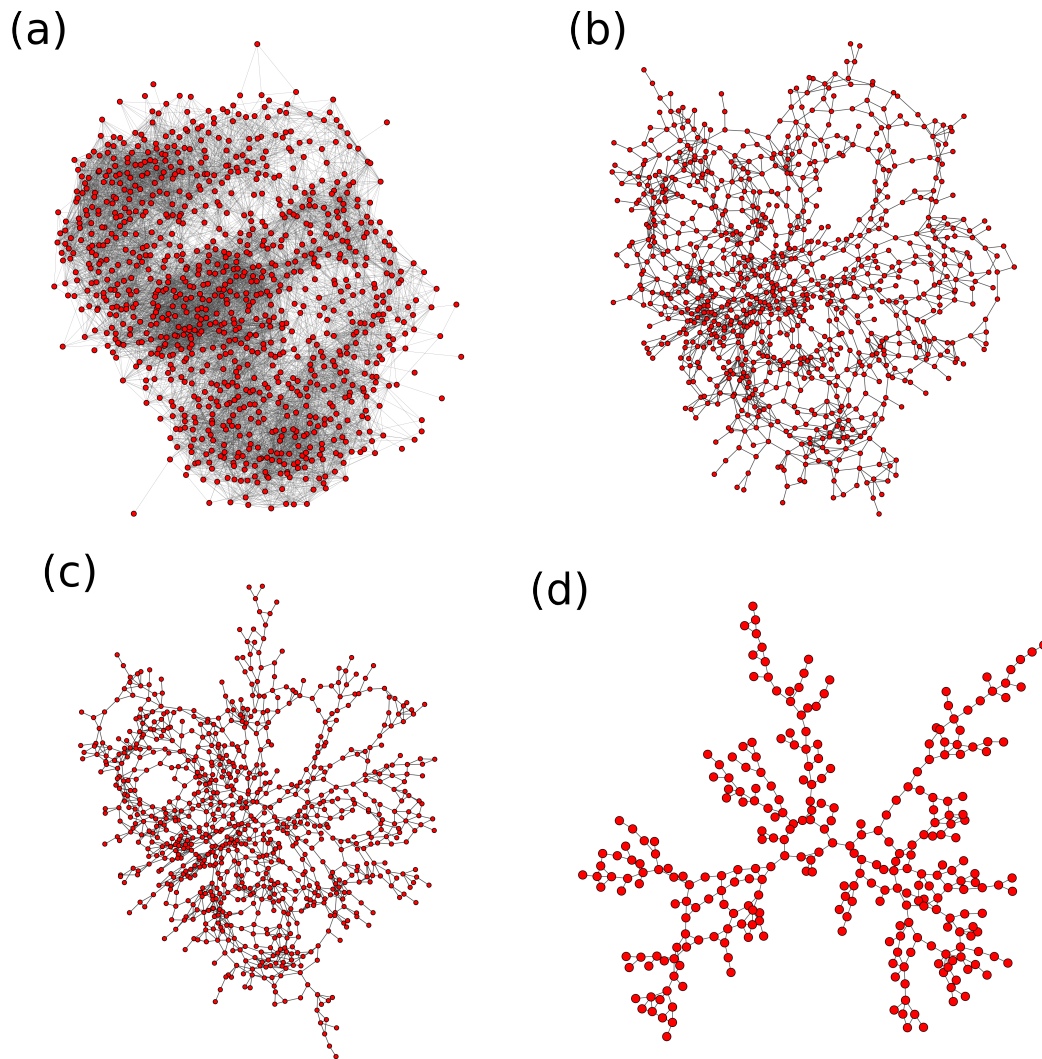


FIG. 19. Human Connectome network Giant cluster network for different threshold values. (a)  $T = 10^{-3}$ , (b)  $T = 3 \cdot 10^{-2}$ , (c)  $T = 3.5 \cdot 10^{-2}$ , and (d)  $T = 6 \cdot 10^{-2}$ . Note that, for the last case, the giant cluster of the network corresponds to a random tree as expected for a usual percolation phase transition.

## REFERENCES

- [1] K. C. Das, The laplacian spectrum, *Comput. Math. Appl.* **48**, 715 (2004).
- [2] S. N. Dorogovtsev and J. F. Mendes, *The nature of complex networks* (Oxford University Press, Oxford, 2022).
- [3] R. Burioni and D. Cassi, Random walks on graphs: ideas, techniques and results, *J. Phys. A* **38**, R45 (2005).
- [4] A. Erzan and A. Tuncer, Explicit construction of the eigenvectors and eigenvalues of the graph laplacian on the cayley tree, *Linear Algebra Its Appl.* **586**, 111–129 (2020).
- [5] H. D. Rozenfeld, S. Havlin, and D. Ben-Avraham, Fractal and transfractal recursive scale-free nets, *New J. Phys.* **9**, 175 (2007).
- [6] T. Vicsek, M. Shlesinger, and M. Matsushita, *Fractals in Natural Sciences* (World Scientific, Singapore, 1994).
- [7] P. Holme and B. J. Kim, Growing scale-free networks with tunable clustering, *Phys. Rev. E* **65**, 026107 (2002).
- [8] F. J. Dyson, Existence of a phase-transition in a one-dimensional ising ferromagnet, *Commun. Math. Phys.* **12**, 91 (1969).
- [9] P. Moretti and M. A. Muñoz, Griffiths phases and the stretching of criticality in brain networks, *Nat. Comm.* **4**, 2521 (2013).
- [10] P. Villegas, T. Gili, G. Caldarelli, and A. Gabrielli, Laplacian renormalization group for heterogeneous networks, *Nat. Phys.* **19**, 445–450 (2023).
- [11] P. Villegas, A. Gabrielli, A. Poggialini, and T. Gili, Multi-scale laplacian community detection in heterogeneous networks, arXiv (2023), 2301.04514.